Korean J. Chem. Eng., 38(3), 498-504 (2021)
DOI: 10.1007/s11814-020-0722-z

pISSN: 0256-1115
eISSN: 1975-7220

Nanocomposites of Fe_2O_3@rGO for adsorptive removal of arsanilic acid from aqueous solution

Li-Li Sui*,†, Li-Na Peng, and Hong-Bo Xu**,†**

*Department of Chemistry, Shenyang Medical College, Shenyang 110034, China
**College of Chemical Engineering, University of Science and Technology Liaoning, Anshan, 114051, China
(*Received 6 June 2020 • Revised 23 November 2020 • Accepted 24 November 2020*)

Abstract−Arsanilic acid (ASA), an organic-arsenic veterinary drug used widely, has greatly attracted attention due to its potential threats. We report the nanocomposites of the α-Fe_2O_3 nanoparticles growth on reduced graphene oxide (rGO) by a one-pot method. The α-Fe_2O_3 nanoparticles are densely covered on the surface of rGO according to the observations of transmission and scanning electron microscope. The adsorptive capacity (357.4±11.2 mg g^{-1}) of the Fe_2O_3@rGO nanocomposites for ASA, which was more than the sum of adsorptive capacities of the pure α-Fe_2O_3 nanoparticles and rGO, revealed a remarkable enhancement due to the synergetic effect of multiple interactions and the good dispersion of α-Fe_2O_3 nanoparticles with more active binding sites in the Fe_2O_3@rGO nanocomposites. The adsorption equilibrium of ASA onto the Fe_2O_3@rGO nanocomposites was achieved for 60 min, and the adsorption of ASA was dependent of pH and temperature, and independent of the concentration of humic acid ranging from 0 to 20 mg L^{-1}. After five cycles of adsorption-desorption, the adsorptive amounts of ASA by the regenerative sorbent still retained 85% of adsorptive amount by the fresh sorbents. The adsorption process of ASA can be described by the Langmuir and the pseudo-second-order equations and is exothermic and spontaneous according to thermodynamic analysis.

Keywords: Arsanilic Acid, Nanocomposites, Graphene, Iron Oxide

INTRODUCTION

Arsanilic acid (4-aminphenylarsonic acid), an organic-arsenic veterinary drug, has been widely employed to promote growth rate, improve feed efficiency and control parasitic diseases for decades in animal-feeding productions [1]. Although the toxicity of arsanilic acid (ASA) is low, the most ingested ASA can be finally excreted in their original form via animal manure and transformed into high toxic inorganic arsenic derivatives under high-moisture and high-temperature conditions during composting [2,3]. The untreated livestock and poultry breeding wastewater enter the soil environment in agriculture, resulting in potential health and environmental risks [4]. Therefore, the effective removal of ASA from the culture wastewater is a crucial requirement for controlling arsenic contamination.

The concentration of ASA in the breeding wastewater is at the level of mg L^{-1} [5]. For the removal of the low-level ASA from the culture wastewater, adsorption is the preeminent method and especially suitable for the treatment of wastewater containing low-concentration pollutants. Some sorbents have been developed for the removal of the organic-arsenic compounds, including metal-organic framework [6], metallic oxide [7], iron (oxyhydr)oxides [8], magnetic greigite [9], molecularly imprinted polymers [10], mineral [11], chitosan [12] and carbon nanotubes [13]. Recently, nanocomposites have exhibited superior performance for the adsorption of organic-arsenic compounds [14-17]. Kong and Wilson [14] reported a binary goethite-cellulose nanocomposite with the advantage of enhanced adsorption of organic-arsenic compound due to the good dispersion of goethite nanoparticles (NPs). Hu et al. [15] developed Fe-modified carbon nanotubes which have higher adsorption capacity of organic-arsenic compound than the unmodified carbon nanotubes due to synergetic effect of multiple interactions. The binary nanocomposites of Fe_3O_4 NPs and reduced graphene oxide (rGO) were developed for the removal of organic-arsenic compounds with higher adsorption capacity compared to the pure Fe_3O_4 NPs and rGO because of the multiple interactions [16,17]. The rGO as the dispersion support of NPs exhibited the highest adsorption capacity of the organic-arsenic compounds because the planar geometry of rGO is amenable modification or functionalization, providing the fabricated adsorbents with the desired properties [18]. Chen and co-workers found that Fe^{3+}, Zn^{2+} and Cu^{2+} dramatically enhanced the adsorption of organic-arsenic compounds on goethite surface [19]. Compared with other metals, Fe^{3+} is a common and cheap element. The α-Fe_2O_3 NPs have been confirmed to be alternative sorbents for the removal of arsenic through the surface As-Fe coordination [20]. Due to the agglomeration of α-Fe_2O_3 NPs, the surface complexation of α-Fe_2O_3 NPs with ASA was weakened. The nanocomposites of the well-dispersed α-Fe_2O_3 NPs on the rGO combine the advantages of α-Fe_2O_3 NPs and rGO, which could improve the adsorptive properties of ASA [21].

In this work, the nanocomposites of Fe_2O_3@rGO were developed and prepared via *in-situ* crystal growth of Fe_2O_3 NPs onto the surface of rGO with hydrothermal process. The objective of this work is to assess the adsorptive process of ASA by the Fe_2O_3@rGO and their possible mechanisms, which would provide an understanding of the role of the Fe_2O_3@rGO for the treatment of ASA

†To whom correspondence should be addressed.
E-mail: sllsqy123@126.com, lnkdxhb@163.com

in the contaminated wastewater.

EXPERIMENTAL

1. Preparation and Characterization of the Fe_2O_3@rGO Nanocomposite

Graphene oxide (GO) was obtained as described in Supporting Information [22]. The product was obtained by centrifugation (16,000 rpm) for 5 min and washing with deionized water to no presence of sulfate ions. Finally, the as-synthesized GO powder was dried at 60 °C for constant weight.

0.40 g of $FeCl_3 \cdot 9H_2O$ was dissolved in 50 mL of ethanol and then the $FeCl_3$ ethanol solution was mixed into 100 mL of the GO suspension aqueous solution (1 g L^{-1}) under magnetic stirring for 15 min. NH_3 solution (30 mL) was mixed dropwise. After the hydrothermal reaction of the mixture at 180 °C for 48 h, the obtained products were isolated by centrifugation (16,000 rpm) for 10 min, washed with methanol, and dried in vacuum at 60 °C overnight. For comparison, the Fe_2O_3 NPs, and the rGO were also prepared using the identical procedure as above. All the reagents and apparatus used are also listed in Supporting Information. The characterization methods are described in Supporting Information.

2. Batch Experiments

The adsorption of ASA on the Fe_2O_3@rGO was tested using batch method. Effect of Fe_2O_3@rGO dosage (1-8 g L^{-1}) on the removal efficiency was tested in ASA solution (20 mL) with 100 mg L^{-1} at pH 5 for 120 min. The ASA solution (20 mL) with varying concentration (100-700 mg L^{-1}) by adding a fixed dose of Fe_2O_3@rGO was stirred for a specified period at desired pH and temperature with stirring rate of 200 rpm. The dosage of the Fe_2O_3@rGO was kept at 4 g L^{-1}. Temperature was adapted to 25, 35 and 45 °C to test the influence of temperature. To measure the influence of contact time on adsorption amounts, the contact time was varied from 10 to 120 min. Influence of pH (3-10) on the removal of ASA was tested at 25 °C for 60 min through modulating solution pH using HCl or NaOH solutions. The typically content of dissolved natural organic matter (DNOM) was below 20 mg L^{-1} in water [23]. The effect of DNOM as humic acid (HA) on the removal efficiency was tested in a solution containing ASA of 100 mg L^{-1} and DNOM of 0, 5, 10, 20 mg L^{-1}. The pH of solution was controlled at pH 9 because HA is water-soluble in alkaline solution. The reuse of the Fe_2O_3@rGO was tested in five cycles of adsorption-desorption using acidic ethanol acidified with 0.1 mol L^{-1} HCl at pH 3 as the eluent according to the previous method [6]. The loaded Fe_2O_3@rGO was added in acidic ethanol with stirring for 6 h, and then the regenerative sorbents were filtrated, washed with deionized water near neutral and dried for the next cycle. All the trials were performed in triplicate and all the measurement data were expressed as the average± standard deviation (SD) at the 5% significance level. After stable situation, the concentration of the ASA in the remnant solution was estimated by a high-performance liquid chromatography (HPLC) method [24]. The adsorptive amount was obtained by Eq. (1) as follows.

$$q=(C_0-C_t)\,V/m \quad (1)$$

where q (mg g^{-1}) is the adsorption capacity, C_0 (mg L^{-1}) is the initial concentration of ASA, C_t (mg L^{-1}) is the remnant concentration of ASA, V (mL) is the volume of solution and m (g) is the mass of Fe_2O_3@rGO nanocomposite.

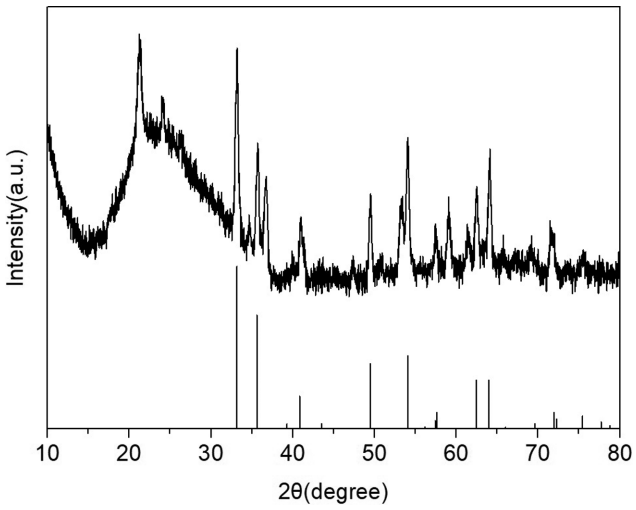

Fig. 1. XRD patterns of the Fe_2O_3@rGO.

RESULTS AND DISCUSSION

1. Characterization

From Fig. 1, the strong and sharp XRD peaks for the crystal phase of well-crystallized Fe_2O_3 NPs are consistent with the peaks of α-Fe_2O_3 particles (JCPDS No. 33-0664) [25], illustrating that the α-Fe_2O_3 particles have been introduced into the hybrid sorbent. Lack of XRD peaks of rGO at 26° is detected due to the overlap of the large amounts of α-Fe_2O_3 particles onto the rGO surface [26].

The 1-D rod-like Fe_2O_3 NPs are formed in the width range of 20-50 nm (Fig. S1(a)) and the well-packed layers of RGO sheets are observed in Fig. S1(b). Large amount coverage of rod-like Fe_2O_3 NPs anchored uniformly on both sides of the rGO sheets can be observed in Fig. 2(a), suggesting the rGO sheets as the stable support for anchoring 1-D Fe_2O_3 NPs. Fe_2O_3 NPs are randomly and well dispersed on the rGO sheets, indicating an efficient assembly between the Fe_2O_3 NPs and rGO sheets during the hydrothermal process. From Fig. 2(b), the SEM image of the Fe_2O_3@rGO agrees with its TEM image and the rod-like Fe_2O_3 NPs are anchored fully on the rGO surface. The presence of a large amount of Fe element in the Fe_2O_3@rGO from the EDS results can confirm the growth of Fe_2O_3 NPs on the rGO surface. The Fe_2O_3@rGO displays the BET surface area of 163 m^2 g^{-1} and pore volume of 0.306 cm^3 g^{-1}. The average pore diameter is estimated to be 0.548 nm. From Fig. 3, the characteristics of Fourier transmission infrared spectrum (such as a band of Fe-O bonds at 571 cm^{-1}, the aromatic C=C stretching vibration at 1,550 cm^{-1}, a shoulder band of the bridging coordinated carboxylates at 1,625 cm^{-1} and a band of carboxyl group at 1,742 cm^{-1}) reveal the presence of Fe_2O_3 and rGO in the Fe_2O_3@rGO [27]. The surface element distribution of the Fe_2O_3@rGO was analyzed by XPS spectrum (Fig. S1). The two peaks at 710.8 and 724.4 eV are assigned to the transitions of Fe 2p3/2 and Fe 2p1/2, which is consistent with hematite phase [28].

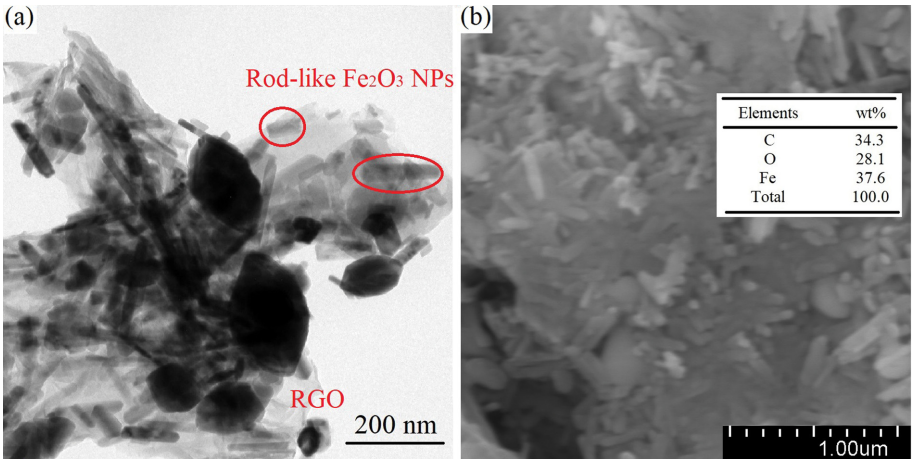

Fig. 2. (a) TEM and (b) SEM images of the Fe_2O_3@rGO.

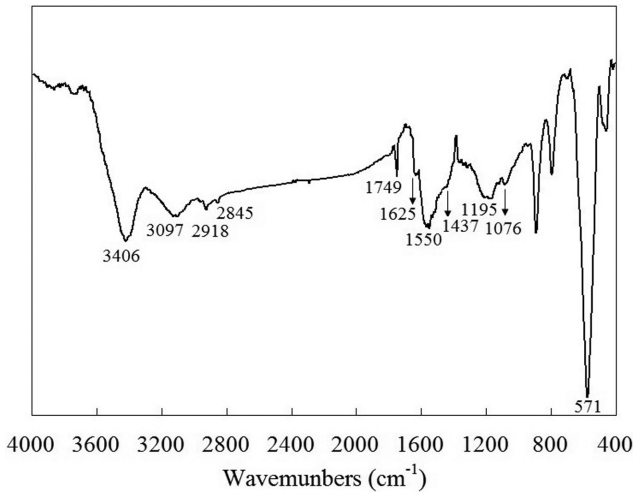

Fig. 3. Fourier transmission infrared spectrum of the Fe_2O_3@rGO.

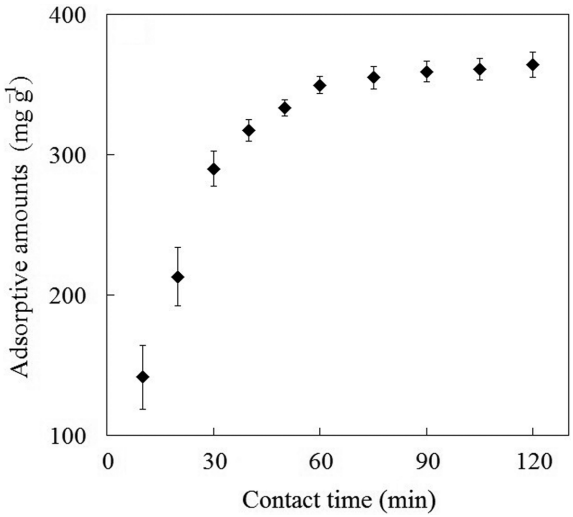

Fig. 4. Effect of contact time.

2. Effect of Fe_2O_3@rGO Dosage

The removal efficiency of ASA in solution increased from 42.4% to 97.2% with the increase in the Fe_2O_3@rGO dosage in the range of 1-4 g L^{-1} (Fig. S2). There was no obvious difference of removal efficiency in the Fe_2O_3@rGO dosage from 5 to 8 g L^{-1}. These results indicate that the Fe_2O_3@rGO dosage of 4 g L^{-1} was sufficient.

3. Effect of Contact Time

The adsorption of ASA by the Fe_2O_3@rGO took place very quickly within the first 30 min (Fig. 4) due to a large amount of available binding sites in the Fe_2O_3@rGO and a large concentration gradient on the interface of solid-liquid at the beginning, and hence the transfer of ASA onto the surface of the Fe_2O_3@rGO was faster. Within the second 30 min, the uptake was slowed because ASA took more time to transport from the surface to internal binding sites. After 60 min, the uptake was settled off and changed insignificantly, indicating that a state of equilibrium was reached. As time increased, the binding sites on the surface of the Fe_2O_3@rGO became exhausted. Our findings were also reported by other researchers, such as a quick uptake of roxarsone in the initial stage by the carbon nanotubes [13] and by the metal-organic frameworks [29]. Therefore, 60 min was suitable as the contact time of ASA adsorption for the subsequent trials.

4. Effect of pH

ASA contains benzene ring, amino group and one arsenic ion with the aqueous dissociation constants (pK_{a1}=1.9 pK_{a2}=4.1 and pK_{a3}=9.2) [7] and there exists the various chemical speciation in the variation of solution pH. The point of zero charge of pH (pH_{PZC}) for the Fe_2O_3@rGO was obtained as in the previous method [30]. The pH_{PZC} of the Fe_2O_3@rGO was 6.7±0.4 according to the pH drift method [30], suggesting that the surface of the Fe_2O_3@rGO was cationic below pH_{PZC} and anionic above pH_{PZC}. The pH-dependence of ASA adsorption is observed as illustrated in Fig. 5. It was found that there was no notable change in the adsorptive amount of ASA by the Fe_2O_3@rGO in the range of pH 3-6 because there was an electrostatic interaction between the negatively charged ASA and the cationic surface of the Fe_2O_3@rGO as the dominant interaction forces. In pH ranging from 6 to 10, the adsorptive amount of ASA by the Fe_2O_3@rGO obviously reduced because of the electrostatic repulsion of the same charged ASA and Fe_2O_3@rGO

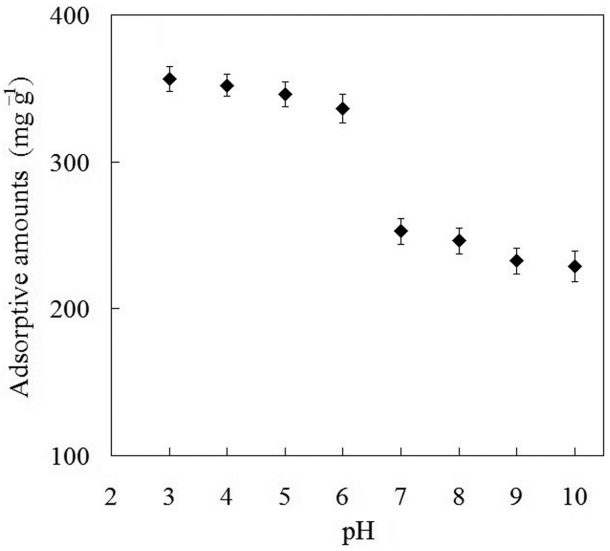

Fig. 5. Effect of pH.

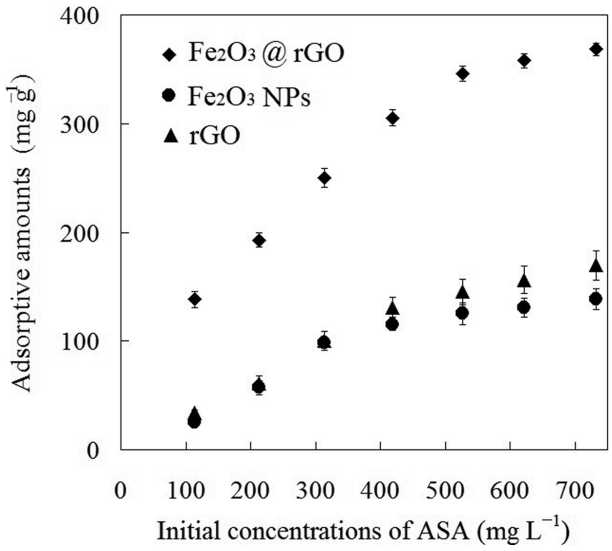

Fig. 6. Effect of the initial ASA concentration.

[31]. Another factor might be that the dissociated species of ASA at high pH inhibited the formation of hydrogen bonds with rGO [15]. These made an unfavorable adsorption of ASA by the Fe_2O_3@rGO at pH>6. However, about 65% of adsorptive amount of ASA at pH≤6 was observed in the pH range of 6-10, illustrating that the in the adsorption of ASA existed other interactions such as (As-Fe coordination) other than electrostatic interactions and/or hydrogen bonds [8,32]. Adamescu and co-workers calculated the binding energy of the As-Fe coordination up to 20 kcal mol^{-1} [33]. Tian and co-workers found that the contribution of the interactions to the adsorption of the organic-arsenic compounds was in the order: As-Fe coordination>hydrogen bonding>π-π interaction [16]. Therefore, the Fe_2O_3@rGO still kept a relatively high adsorptive amount at pH>6 due to the stable interaction of As-Fe coordination. Similar results had been exhibited by other research [6,34]. Therefore, the pH of 5 was used as the desired pH for the ASA adsorption in the subsequent trials.

5. Adsorbed Amounts

As the initial concentration enhanced, the adsorptive amount of ASA by the Fe_2O_3 NPs, the pure rGO and the Fe_2O_3@rGO increased (Fig. 6). The Fe_2O_3@rGO was used as an example, and the adsorptive amount of ASA was dependent on the ASA concentrations from 100 to 500 mg L^{-1} in feed solution. After 500 mg L^{-1}, a small variation in the adsorptive amount of ASA by the Fe_2O_3@rGO was exhibited. The experimental values of the adsorptive amount of ASA by the Fe_2O_3 NPs, the rGO and the Fe_2O_3@rGO were found to be 127.5±6.7, 150.5±12.3 and 357.4±11.2 mg g^{-1}, respectively. The adsorptive amount of ASA by the Fe_2O_3@rGO was more than the sum of adsorptive amounts of the Fe_2O_3 NPs and the rGO. This phenomenon is attributed to (1) the synergetic effect of multiple interactions of Fe_2O_3@rGO with ASA (such as electrostatic force, hydrogen bonding, As-Fe coordination and π-π interaction) [16], (2) the good dispersion of Fe_2O_3 NPs on the rGO in the hybrid process which is a benefit for the formation of As-Fe surface coordination [35,36], and (3) the formation of more active binding sites of the Fe_2O_3@rGO. These factors led to a notable increase in the adsorption amount of ASA by the Fe_2O_3@rGO compared with the Fe_2O_3 NPs and the rGO. Similar phenomena were also described for other nanocomposites [16,17]. There was a comparison of the Fe_2O_3@rGO nanocomposites in the adsorptive amount of ASA with previously reported sorbents as listed in Table 1 [6,8,17,32,36-38]. The Fe_2O_3@rGO nanocomposites has relatively high adsorptive amounts and relatively rapid adsorptive rate compared with most of previously reported sorbents. Fig. S3 displays that the presence of HA has no significant matrix effect. Inhibition influence on the removal efficiency of ASA was not ob-

Table 1. Comparison of various sorbents toward ASA adsorption

Sorbents	Capacity (mg g^{-1})	Contact time	Ref.
Zeolitic imidazolate framework-8	791.1	6 h	[6]
Iron (oxyhydr) oxides	156.3	5 h	[8]
Fe_3O_4@RGO	313.7	15 min	[17]
Metal-organic frameworks	302.3	3 h	[31]
Goethite	213.6	5 h	[35]
Iron humate	188.7	5 h	[36]
MgO	86.8	7 h	[37]
Fe_2O_3@RGO	357.4	60 min	This work

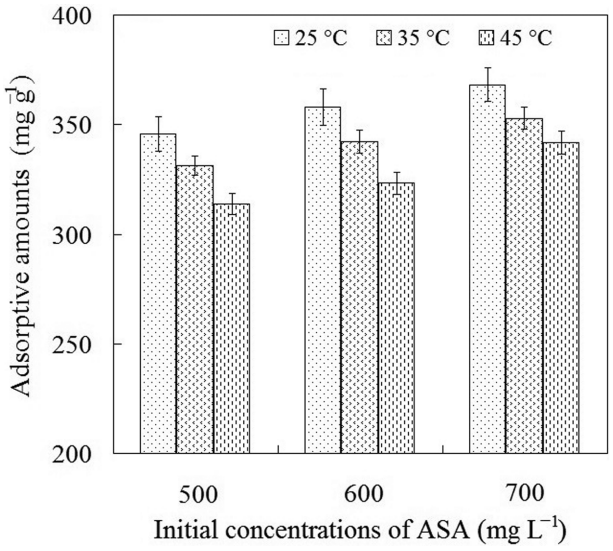

Fig. 7. Effect of temperature.

Table 2. Isotherms parameters for the adsorption of ASA at 25 °C

Langmuir	Freundlich	D-R
q_{max}=423.7 mg g^{-1}	K_F=19.81 L g^{-1}	k_{ad}=0.0049 mol^2 kJ^{-2}
b=0.01145 L mg^{-1}	1/n=0.471	q_s=1,517.8 mg g^{-1} E=10.1 mol kJ^{-1}
R^2=0.9991	R^2=0.9866	R^2=0.9921

served as the HA concentration ranged from 0 to 20 mg L^{-1}. Due to the formation of firm bond via surface coordination of ASA with the Fe_2O_3@rGO, ASA was not suffering the competitive adsorption with HA on the surface of Fe_2O_3@rGO.

6. Effect of Temperature

The adsorptive amount of ASA by the Fe_2O_3@rGO decreased slightly with the increase of temperature 25-45 °C (Fig. 7), indicating that the adsorption of ASA was exothermic and a higher temperature was unfavorable for the adsorption of ASA. The exothermic characteristics of the Fe_2O_3@rGO for the ASA adsorption could be attributed to the fact that the complexation of As-Fe and the π-π interaction between rGO and ASA were exothermic reactions [13,33]. Similar trends were found by the previous reports [15,16].

7. Adsorption Isotherm

The equilibrium data were further fitted with three adsorption isotherms: Langmuir, Freundlich and Dubinin-Radushkevich (D-R) [39,40]. The fitting equations of these isotherms are described in Supporting Information. From Table 2 and Fig. S5, the R^2 values from Langmuir (0.9991) and D-R (0.9921) models are higher than that from Freundlich (0.9866) model, illustrating that the ASA adsorption maybe follows the Langmuir and D-R models. Moreover, the theoretical maximum adsorption amount of ASA from Langmuir model was found to be 423.7 mg g^{-1} and closer to the experimental value than the theoretical value from D-R model of 1,517.8 mg g^{-1}, illustrating that Langmuir model is more suitable to reflect the feature of the ASA adsorption on the Fe_2O_3@rGO with a higher reliability. The E value from D-R model was calculated to be 10.1 mol kJ^{-1}, which follows the energetic range of chemical adsorption [41], illustrating that the chemical interaction between ASA and the Fe_2O_3@rGO may occur during the adsorptive process [42]. In brief, the Langmuir model provides a more representative description for the ASA adsorption by the Fe_2O_3@rGO.

Table 4. Thermodynamic parameters for adsorption of ASA

Thermodynamic constants	Temperature (°C)		
	25	35	45
lnb	9.35	9.19	9.14
ΔG^o (kJ mol^{-1})	−23.16	−23.54	−24.15
ΔH^o (kJ mol^{-1})		−8.38	
ΔS^o (J mol^{-1} K^{-1})		49.47	

8. Kinetic Study

The data were also fitted with three kinetic models (such as pseudo-first-order (PFO), pseudo-second-order (PSO) and Elovich models) [43]. The fitting kinetic equations are described in Supporting Information. According to Table 3 and Fig. S6, the R^2 values from PFO and Elovich equations were found to be 0.9626 and 0.9176, respectively, which were lower than that obtained from the PSO equation (0.9948), demonstrating that the PFO and Elovich plots were not satisfactory for fitting the kinetic data. In addition, the q_{eq} value calculated of ASA from the PSO equation is nearly consistent with the experimental value, while the q_{eq} value calculated of ASA from the PFO equation is significantly lower than its experimental value. Therefore, the PSO model can well represent the kinetic process of ASA adsorption by the Fe_2O_3@rGO.

9. Thermodynamic Study

The thermodynamic parameters were calculated using the equations as listed in Supplementary Material. The standard enthalpy change (ΔH^o), the standard entropy change (ΔS^o) and the change in standard free energy of Gibbs (ΔG^o) were calculated as described previously (as listed in Table 4) [44]. The value of ΔG^o at 25, 35 and 45 °C was found to be −19.4, −19.6 and −20.1 kJ mol^{-1}, respectively, confirming the feasibility and spontaneity of the ASA adsorption by the Fe_2O_3@rGO [45]. The negative value of ΔH^o (−8.4 kJ mol^{-1}) revealed that the uptake of ASA was exothermic, suggesting that a low temperature in the tested range was more favorable for the adsorption of ASA, which was in accordance with the results obtained from Fig. 3(d). The positive value of ΔS^o (36.8 J

Table 3. Calculated kinetic parameters for the adsorption of ASA

Pseudo-first-order	Pseudo-second-order	Elovich
k_1=0.034 min^{-1}	k_2=0.18×10^{-3} g mg^{-1} min^{-1}	α=246.5 mg g^{-1} min^{-1}
q_{eq}(cal)=208.9 mg g^{-1}	q_{eq}(cal)=416.7 mg g^{-1}	β=0.023 g^{-1} mg
R^2=0.9626	R^2=0.9948	R^2=0.9176

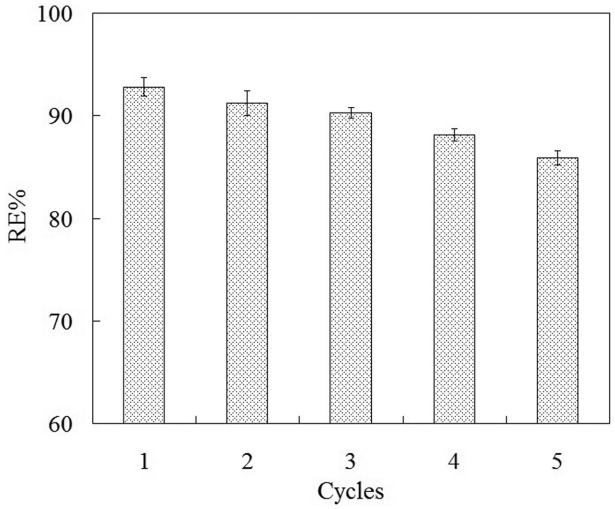

Fig. 8. Reusability of the regenerated Fe_2O_3@RGO.

mol^{-1} K^{-1}) suggested the increase of randomness, which might be attributed to the desorption of several molecules of solvent as each molecule of ASA adsorbed [46]. Similar results were also observed in previous literature [6,47].

10. Reusability

Five cycles of the adsorption-desorption were carried out to test the reusability of the Fe_2O_3@rGO (Fig. 8). The regenerative efficiency (RE) can be calculated by Eq. (2) as follows:

$$RE\ \% = (Q_{Regenerated}/Q_{Fresh}) \times 100\% \quad (2)$$

where $Q_{Regenerated}$ (mg g^{-1}) is an adsorptive amount of ASA by the regenerative Fe_2O_3@rGO, and Q_{Fresh} (mg g^{-1}) is an adsorptive amount of ASA by the fresh Fe_2O_3@rGO. The values of ER% decreased slightly with the increase of in cycle numbers. The adsorptive amounts of ASA by the regenerative Fe_2O_3@rGO were close to 85% of the fresh Fe_2O_3@rGO, indicating that the Fe_2O_3@rGO was a reusable sorbent and could be recycled. The concentration of Fe ions in the eluent was not detected by flame atomic absorption spectrometry, indicating that there was no notable Fe leach from the Fe_2O_3@rGO during the process of elution.

CONCLUSION

A nanocomposite of the Fe_2O_3@rGO with the good performance of the ASA adsorption was prepared. The Fe_2O_3@rGO nanocomposites had better-adsorbed amounts, faster-adsorbed rate and good reusability. The higher adsorptive amount of ASA by the Fe_2O_3@rGO was observed in the range of pH 3-6. The adsorption amount of ASA by the Fe_2O_3@rGO was improved significantly due to the synergetic effect of multiple interactions, the good dispersion of Fe_2O_3 NPs on the surface of rGO and the formation of more active binding sites. There was no significant inhibition influence of HA on the removal efficiency of ASA in the range of HA from 0 to 20 mg L^{-1}. A decrease in the adsorptive amount of ASA by the Fe_2O_3@rGO was found with the increase in temperature during 25-45 °C due to its exothermicity. The ASA adsorption followed well the Langmuir and PSO models and was a spontaneous process.

ACKNOWLEDGEMENTS

Financial support of this work was provided by the Science and technology development fund of Shenyang Medical College (20191026) and by scientific research foundation of education department of Liaoning province (LN201902).

SUPPORTING INFORMATION

Additional information as noted in the text. This information is available via the Internet at http://www.springer.com/chemistry/journal/11814.

REFERENCES

1. L. R. Overby and S. Lilian, *Toxicol. Appl. Pharmacol.*, **7**, 850 (1965).
2. D. W. Rutherford, A. J. Bednar, J. R. Garbarino, R. Needham, K. W. Staver and R. L. Wershaw, *Environ. Sci. Technol.*, **37**, 1515 (2003).
3. J. R. Garbarino, A. J. Bednar, D. W. Rutherford, R. S. Beyer and R. L. Wershaw, *Environ. Sci. Technol.*, **37**, 1509 (2003).
4. B. L. Brown, A. D. Slaughter and M. Schreiber, *Appl. Geochem.*, **20**, 123 (2005).
5. J. Xu, X. Shen, D. Wang, C. Zhao, Z. Liu, I. P. Pozdnyakov, F. Wu and J. Xia, *Chem. Eng. J.*, **336**, 334 (2018).
6. B. K. Jung, J. W. Jun, Z. Hasan and S. H. Jhung, *Chem. Eng. J.*, **267**, 9 (2015).
7. S. Chen, J. Deng, C. Ye, C. Xu, L. Huai, J. Li and X. Li, *Sci. Total Environ.*, **742**, 140587 (2020).
8. T. P. Joshi, G. Zhang, R. Koju, Z. Qi, R. Liu, H. Liu and J. Qu, *Sci. Total Environ.*, **601-602**, 713 (2017).
9. W. Liu, Z. Ai, R. A. Dahlgren, L. Zhang and X. Wang, *Chem. Eng. J.*, **330**, 1232 (2017).
10. W. Fan, X. Zhang, Y. Zhang, P. Wang, L. Zhang, Z. Yin, J. Yao and W. Xiang, *J. Mol. Recognit.*, **31**, e2625 (2018).
11. Y.-J. Wang, F. Ji, W. Wang, S.-J. Yuan and Z.-H. Hu, *Desalin. Water Treatm.*, **57**, 20520 (2016).
12. L. Poon, S. Younus and L. D. Wilson, *J. Colloid Interface Sci.*, **420**, 136 (2014).
13. J. Hu, Z. Tong, Z. Hu, G. Chen and T. Chen, *J. Colloid Interface Sci.*, **377**, 355 (2012).
14. D. Kong and L. D. Wilson, *Carbohyd. Polym.*, **169**, 282 (2017).
15. J. Hu, Z. Tong, G. Chen, X. Zhan and Z. Hu, *Int. J. Environ. Sci. Technol.*, **11**, 785 (2014).
16. C. Tian, J. Zhao, J. Zhang, S. Chu, Z. Dang, Z. Lin and B. Xing, *Environ. Sci.: Nano*, **4**, 2134 (2017).
17. N. You, X.-F. Wang, J.-Y. Li, H.-T. Fan and Q. Zhang, *J. Ind. Eng. Chem.*, **70**, 346 (2019).
18. T. A. Saleh, M. M. Al-Shalalfeh and A. A. Al-Saadi, *Sensors Actuat. B: Chem.*, **254**, 1110 (2018).
19. L. Y. Wang, S. W. Wang and W. R. Chen, *Chemosphere*, **152**, 423 (2016).
20. W. Tang, Q. Li, S. Gao and J. K. Shang, *J. Hazard. Mater.*, **192**, 131 (2011).
21. X. Zhao, L. Lv, B. Pan, W. Zhang, S. Zhang and Q. Zhang, *Chem. Eng. J.*, **170**, 381 (2011).
22. W. S. Hummers and R. E. Offeman, *J. Am. Chem. Soc.*, **80**, 1339

(1958).
23. N. You, Y. Chen, Q.-X. Zhang, Y. Zhang, Z. Meng and H.-T. Fan, *Sci. Total Environ.*, **735**, 139553 (2020).
24. F.-F. Zhang, W. Wang, S.-J. Yuan and Z.-H. Hu, *J. Hazard. Mater.*, **279**, 562 (2014).
25. M. Sun, H. Liu, Y. Liu, J. Qu and J. Li, *Nanoscale*, **7**, 1250 (2015).
26. K. Urbas, M. Aleksandrzak, M. Jedrzejczak, M. Jedrzejczak, R. Rakoczy, X. Chen and E. Mijowska, *Nanoscale Res. Lett.*, **9**, 656 (2014).
27. C. Z. Zhu, S. J. Guo, Y. X. Fang and S. J. Dong, *ACS Nano*, **4**, 2429 (2010).
28. C. Wu, H. Zhang, Y. X. Wu, Q. C. Zhuang, L. L. Tian and X. X. Zhang, *Electrochim. Acta*, **134**, 18 (2014).
29. B. Li, X. Zhu, K. Hu, Y. Li, J. Feng, J. Shi and J. Gu, *J. Hazard. Mater.*, **302**, 57 (2016).
30. I. I. Salame and T. J. Bandosz, *J. Colloid Interface Sci.*, **240**, 252 (2001).
31. J. Deng, Y.-J. Chen, Y.-A. Lu, X.-Y. Ma, S.-F. Feng, N. Gao and J. Li, *Environ. Sci. Pollut. Res.*, **24**, 14396 (2017).
32. J. W. Jun, M. Tong, B. K. Jung, Z. Hasan, C. Zhong and S. H. Jhung, *Chem. Eur. J.*, **21**, 347 (2015).
33. A. Adamescu, I. P. Hamilton and H. A. Al-Abadleh, *J. Phys. Chem. A*, **118**, 5667 (2014).
34. T. Sun, Z. Zhao, Z. Liang, J. Liu, W. Shi and F. Cui, *Chem. Eng. J.*, **334**, 1527 (2018).
35. W. Mitchell, S. Goldberg and H. A. Al-Abadleh, *J. Colloid Interface Sci.*, **358**, 534 (2011).
36. W. R. Chen and C. H. Huang, *J. Hazard. Mater.*, **227-228**, 378 (2012).
37. Y. Peng, W. Wei, H. Zhou, S. Ge, S. Li, G. Wang and Y. Zhang, *J. Dispers. Sci. Technol.*, **37**, 1590 (2016).
38. T. P. Joshi, G. Zhang, H. Cheng, R. Liu, H. Liu and J. Qu, *Water Res.*, **116**, 126 (2017).
39. H.-T. Fan, J.-B. Wu, X.-L. Fan, D.-S. Zhang, Z.-J. Su, F. Yan and T. Sun, *Chem. Eng. J.*, **198-199**, 355 (2012).
40. H.-T. Fan, X.-T. Sun, Z.-G. Zhang and W.-X. Li, *J. Chem. Eng. Data*, **59**, 2106 (2014).
41. H. Javadian, P. Vahedian and M. Toosi, *Appl. Surf. Sci.*, **284**, 13 (2013).
42. H.-T. Fan, Q. Tang, Y. Sun, Z.-G. Zhang and W.-X. Li, *Chem. Eng. J.*, **258**, 146 (2014).
43. H.-T. Fan, X.-T. Sun and W.-X. Li, *J. Sol-Gel Sci. Technol.*, **72**, 144 (2014).
44. Y. Liu, *J. Chem. Eng. Data*, **54**, 1981 (2009).
45. H.-T. Fan, W. Sun, B. Jiang, Q.-J. Wang, D.-W. Li, C.-C. Huang, K.-J. Wang, Z.-G. Zhang and W.-X. Li, *Chem. Eng. J.*, **286**, 128 (2016).
46. H. Fan, X. Fan, J. Li, M. Guo, D. Zhang, F. Yan and T. Sun, *Ind. Eng. Chem. Res.*, **51**, 5216 (2012).
47. H.-T. Fan, Y. Sun, Q. Tang, W.-L. Li and T. Sun, *J. Taiwan Inst. Chem. Eng.*, **45**, 2640 (2014).

Supporting Information

Nanocomposites of Fe_2O_3@rGO for adsorptive removal of arsanilic acid from aqueous solution

Li-Li Sui*,†, Li-Na Peng, and Hong-Bo Xu**,†**

*Department of Chemistry, Shenyang Medical College, Shenyang 110034, China
**College of Chemical Engineering, University of Science and Technology Liaoning, Anshan, 114051, China
(*Received 6 June 2020 • Revised 23 November 2020 • Accepted 24 November 2020*)

Materials

Graphite powder was purchased from Qingdao Xiyou Fine Graphite Chemical Co., LTD (Qingdao, China). All the other reagents were at least of analytical grade and obtained from Sinopharm Chemical Reagent Co., Ltd (Shanghai, China).

Characterization

The product obtained was characterized by X-ray diffraction using Cu Kα radiation (XRD, Almelo PW-3060, Netherland), A Shimadzu SSX-550 scanning electron microscope (SEM) combined with an energy-dispersive X-ray spectroscopy (EDS), and TECNAI G20 transmission electron microscope (TEM, FEI, USA). The absorption spectra of the samples were taken at room temperature by a Nicolet 6700 Fourier transmission infrared spectroscopy (FT-IR) in the range of 400-4,000 cm^{-1} with a resolution of 1 cm^{-1} using KBr window and a BWS465-785S laser confocal Raman spectroscopy (B&W Tek LLC, USA). The chemical environment of the surface composition of the Fe_2O_3@rGO nanocomposites was recorded by Thermo Scientific ESCALAB 250Xi X-ray photoelectron spectroscopy (XPS, Thermo, Waltham, USA). Textural characterization of the adsorbents was accomplished by N_2 adsorption-desorption isotherms at 77 K.

Analysis

The concentrations of ASA were determined by high-performance liquid chromatography (HPLC) at 264 nm with C_{18} column using the mixture solution of 0.05 mol L^{-1} KH_2PO_4 containing 0.1% formic acid (v/v) and methanol in a 95 : 5 (v/v) ratio with a flow rate of 1.0 mL min^{-1} at 30 °C.

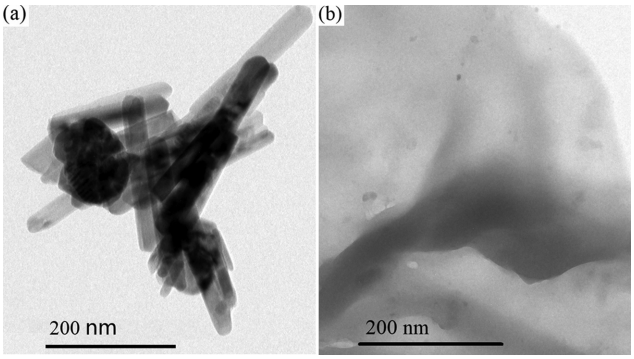

Fig. S1. TEM images of (a) Fe_2O_3 NPs and (b)RGO.

Calculation of adsorption capacity

$$q=(C_0-C_t)\ V/m \quad \text{(S1)}$$

where q (mg g^{-1}) is the adsorption capacity, C_0 (mg L^{-1}) is the ini-

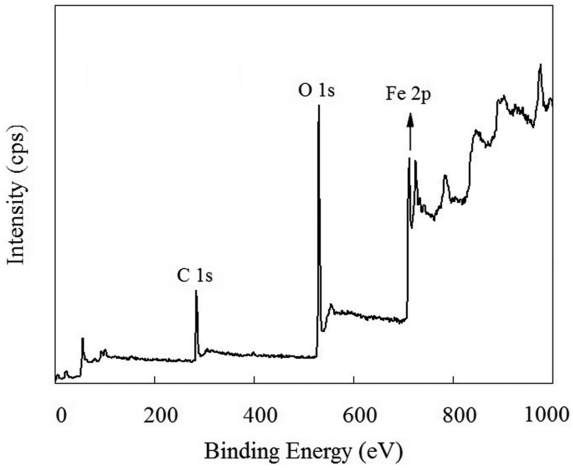

Fig. S2. Wide scan XPS spectrum of the Fe_2O_3@rGO.

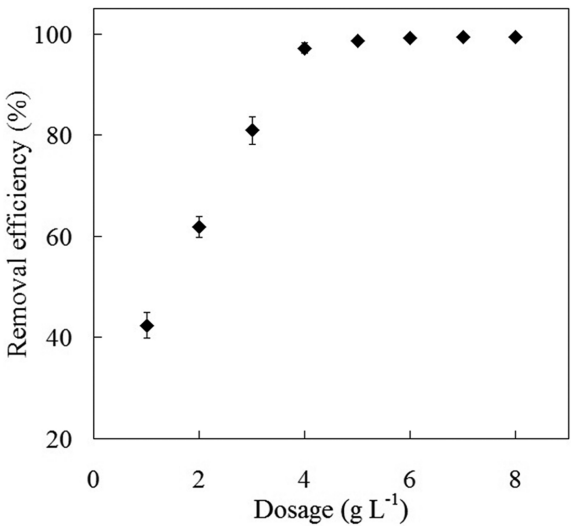

Fig. S3. Effect of dosage.

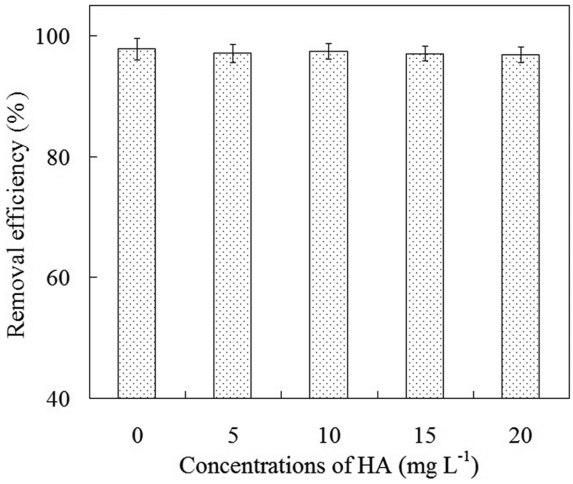

Fig. S4. Effect of HA.

tial concentration of ASA, C_t (mg L^{-1}) is the remnant concentration of ASA, V (mL) is the volume of solution and m (g) is the mass of Fe_2O_3@rGO nanocomposite.

Adsorption isotherms

The linearized equations of Langmuir, Freundlich and Dubinin-Radushkevich (D-R) isotherm can be expressed as Eqs. (S1) and (S2), respectively.

$$C_e/q_e = 1/(q_{max}\, b) + C_e/q_{max} \quad \text{(S2)}$$

$$\log q_e = \log k_F + (1/n) \log C_e \quad \text{(S3)}$$

$$\ln q_e = \ln q_s - k_{ad}\varepsilon^2 \quad \text{(S4)}$$

where q_e (mg g^{-1}) is the amount of Ca^{2+} ions adsorbed per unit mass of BCES at equilibrium; C_e (mg L^{-1}) is the concentration at equilibrium; q_{max} (mg g^{-1}) is the maximum adsorption at monolayer coverage; b (L mg^{-1}) is the adsorption equilibrium constant; K_F (L g^{-1}) is a Freundlich constant; n is a constant; k_{ad} (mol^2 kJ^{-2}) is the D-R isotherm constant; q_s (mg g^{-1}) is the saturation capacity from D-R isotherm; ε is the Polanyi potential and calculated as follows:

$$\varepsilon = RT \ln (1 + 1/C_{eq}) \quad \text{(S5)}$$

where R (8.314 J mol^{-1} K^{-1}) is universal gas constant; T (K) is the absolute temperature. C_{eq} (mol L^{-1}) is the equilibrium concentration of adsorbate.

E (kJ mol^{-1}) is the change of free energy transforming 1 mol of adsorbates from solution to the surfaces and is conducive to the estimation of adsorption reaction type, and is obtained from k_{ad} as

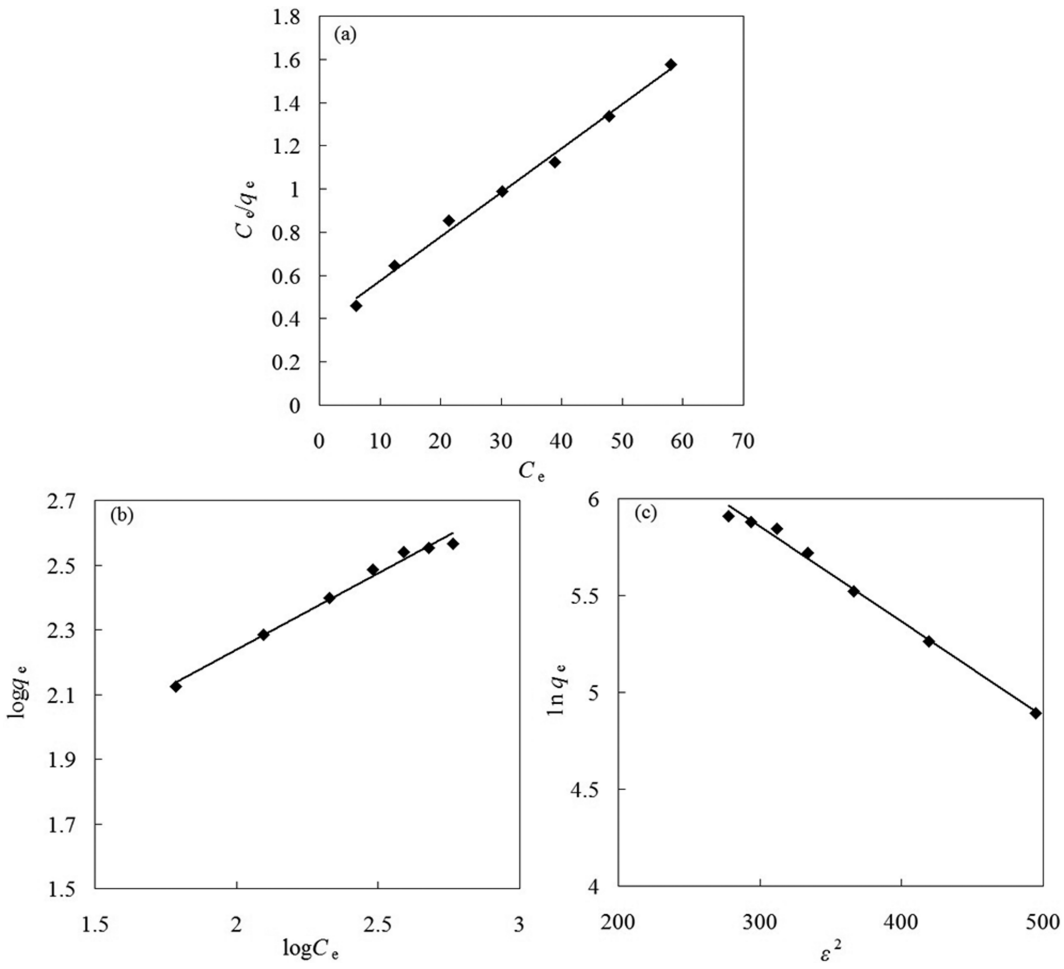

Fig. S5. Fitting plots of adsorption isotherm: (a) Langmuir, (b) Frendlich and (c) D-R.

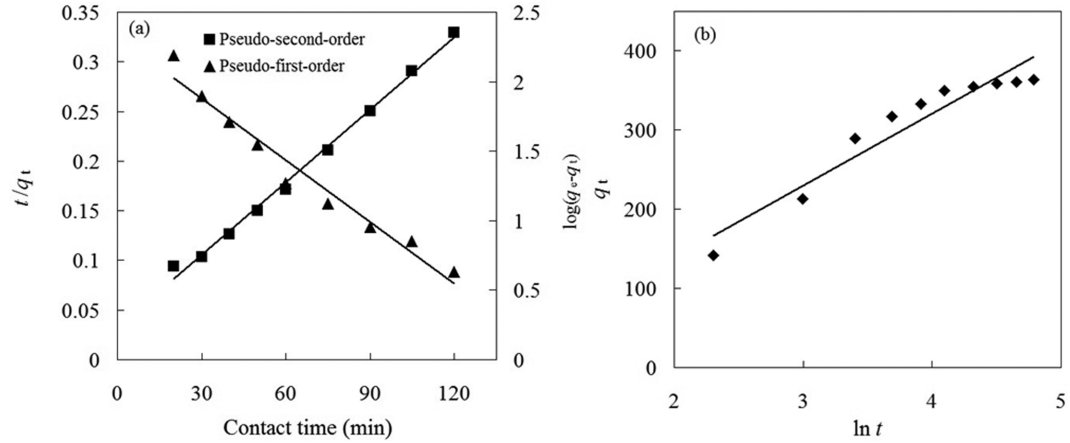

Fig. S6. Fitting plots of adsorption kinetic: (a) Pseudo-first-order, (b) pseudo-second-order and (c) Elovich equations.

follows:

$$E=-(2k_{ad})^{-1/2} \quad (S6)$$

Kinetic analysis

The pseudo-first-order, pseudo-second-order and Elovich rate expressions are linearly expressed as:

$$\log(q_e-q_t)=\log q_e-k_1t/2.303 \quad (S7)$$

$$t/q_t=1/k_2q_e^2+t/q_e \quad (S8)$$

$$q_t=(1/\beta)\ln(a\beta)+(1/\beta)\ln t \quad (S9)$$

where k_1 (min^{-1}) is the rate constant of the pseudo-first-order adsorption. q_e and q_t (mg g^{-1}) are the adsorption capacity at equilibrium and the adsorption amount at time t (min), respectively. k_2 (g mg^{-1} min^{-1}) is the rate constant of the pseudo-second-order equation. α is the initial adsorption rate of Elovich equation (mg·g^{-1}·min^{-1}) and β is related to the extent of surface coverage and activation energy for chemisorption.

Thermodynamic analysis

Thermodynamic parameters such as standard Gibbs free energy change (ΔG^o), enthalpy change (ΔH^o) and entropy change (ΔS^o) at equilibrium at different temperatures can be calculated from the constant (b, L mol^{-1}) of Langmuir isotherm equation as the following equations:

$$\Delta G^o=-RT\ln b \quad (S10)$$

In order to use b in the thermodynamic calculations, the value of b expressed in L mg^{-1} in Langmuir isotherm equation can be multiplied by 1,000 to convert the units in L g^{-1}, and then multiplied by the molecular weight of the ASA (M_r=217.06), to transform b in L mol^{-1}.

ΔH^o and ΔS^o were obtained from Eq. (S11).

$$\ln b=\frac{\Delta S^o}{R}-\frac{\Delta H^o}{RT} \quad (S11)$$